

Tracking pulsar dispersion measures using the GMRT

A. L. Ahuja,¹ Y. Gupta,² D. Mitra,² and A. K. Kembhavi¹

¹ IUCAA, Ganeshkhind, Pune University, Pune, India

² National Centre for Radio Astrophysics, TIFR, Pune University Campus, Pune 411007, India

Released 2004 Xxxxx XX

ABSTRACT

In this paper, we describe a novel experiment for the accurate estimation of pulsar dispersion measures using the Giant Metre-wave Radio Telescope. This experiment was carried out for a sample of twelve pulsars, over a period of more than one year (January 2001 to May 2002) with observations about once every fortnight. At each epoch, the pulsar DMs were obtained from simultaneous dual frequency observations, without requiring any absolute timing information. The DM estimates were obtained from both the single pulse data streams and from the average profiles. The accuracy of the DM estimates at each epoch is ~ 1 part in 10^4 or better, making the data set useful for many different kinds of studies.

The time series of DM shows significant variations on time scales of weeks to months for most of the pulsars. A comparison of the mean DM values from these data show significant deviations from catalog values (as well as from other estimates in literature) for some of the pulsars, with PSR B1642–03 showing the most notable changes. From our analysis results it appears that constancy of pulsar DMs (at the level of 1 in 10^3 or better) can not be taken for granted. For PSR B2217+47, we see evidence for a large-scale DM gradient over a one year period, which is modeled as being due to a blob of enhanced electron density sampled by the line of sight. For some pulsars, including pulsars with fairly simple profiles like PSR B1642–03, we find evidence for small changes in DM values for different frequency pairs of measurement, a result that needs to be investigated in detail. Another interesting result is that we find significant differences in DM values obtained from average profiles and single pulse data.

Key words: miscellaneous – methods:data analysis – pulsars: general – H_{II} regions.

1 INTRODUCTION

The radio signals from a pulsar suffer dispersion as they travel through the ionized component of the inter-stellar medium (ISM), resulting in a frequency dependent arrival time of the pulses. The effect is quantified by the pulsar’s dispersion measure (DM), defined as the integral of the electron column density along the line of sight,

$$DM = \int_0^L n_e dl \text{ pc/cm}^3 \quad (1)$$

The delay between the pulse arrival time at two frequencies, Δt , can then be expressed as

$$\Delta t = K \left(\frac{1}{f_1^2} - \frac{1}{f_2^2} \right) DM \quad , \quad (2)$$

where

$$K = \frac{e^2}{2\pi mc} = \frac{1}{2.410331 \times 10^{-4}} \text{ MHz}^2 \text{ cm}^3 \text{ s/pc} \quad . \quad (3)$$

Here Δt is in units of second for f_1 and f_2 in MHz and DM in the traditional units of pc/cm^3 . The precise value of the constant K is as given in Backer et al. (1993).

The DM of a pulsar is a basic parameter, and its value needs to be known with sufficient accuracy for proper dispersion correction to be carried out on the received signal. Further, accurate estimates of DM can be used to probe the pulsar emission geometry (e.g. Kardashev et al. 1982). Estimates of DM obtained from different values of f_1 and f_2 in Equation 2 have been used to check the validity of the cold plasma dispersion relation for the ISM (e.g. Phillips & Wolszczan 1992, and references therein). In addition, small variations in a pulsar’s DM are expected due to random electron density fluctuations in the ISM, thought to be associated with turbulence in the medium. Such variations, expected on relatively large time-scales of weeks to months, have indeed been observed (e.g. Backer et al. 1993; Phillips & Wolszczan 1991). Pulsar dispersion monitoring thus provides a direct method for probing the structure of the spectrum of electron density fluctuations.

Though first order estimates of the DM can be obtained by careful measurements of the arrival time delays in a multi-channel receiver operating at a single wave-band (e.g. during the pulsar search and discovery process itself) the more accurate estimates needed for the applications discussed above require more sophisticated experiments. Typically, refined pulsar DMs (and their variations with epoch) are estimated as part of the analysis of multi-epoch multi-frequency timing data from an observatory (e.g. Backer et al. 1993; Phillips & Wolszczan 1992). An alternate method is to conduct simultaneous dual frequency observations at f_1 and f_2 and estimate the DM from a measure of the arrival time delay, using Equation 2 (e.g. Bartel et al. 1981; Kardashev et al. 1982; Hankins 1987). The advantage of this method is that observations at a single epoch are self-sufficient for obtaining the DM at that epoch and the DM is obtained more directly, rather than as one of the parameters in a multi-parameter timing solution. For single dish telescopes, this method requires simultaneous operation of receivers at more than one wave-band; alternatively, different single dish telescopes can be configured at each wave-band while simultaneously observing the same pulsar.

In this paper, we describe a new experiment for accurate estimation of pulsar DMs, using the Giant Metre-wave Radio Telescope (GMRT) in a simultaneous multi-frequency pulsar observation mode. Section 2 describes the details of the experiment and the observation strategy. Section 3 gives the details of the data reduction, and describes the technique used for estimating DMs from the reduced data. The main results and the possibilities for follow-up work are described in Section 4.

2 A NEW EXPERIMENT FOR MEASURING DM

The accuracy of the DM estimate depends on the precision to which the time delay between the pulse profiles at two frequencies can be measured. If Δt_{rms} is the error on the measurement of the time delay, then the fractional DM error is

$$\frac{DM_{rms}}{DM} = \frac{\Delta t_{rms}}{\Delta t} \quad (4)$$

For a given value of Δt_{rms} (which is usually limited by the S/N of the data at the two frequencies, or sometimes by the coarseness of the sampling interval), it is clear that the greater the relative time delay between the arrival of signals at the two frequencies, Δt , the more accurate is the DM estimate. This would favour large separations between the two observing radio bands. However, if the pulsar profile evolves significantly over this range of frequencies, then it can bias the measured Δt , leading to an error in the estimate of the DM. This effect favours a smaller separation between the two radio wave-bands. Also, according to Equation 2, for a given separation between a pair of radio bands f_1 and f_2 , smaller values of frequencies give a larger value of estimated Δt , and in turn, a better accuracy for final DM estimation. The final choice of the two frequency bands of operations is then decided by these considerations. Other requirements for obtaining accurate DM estimates are (a) high signal to noise ratio stable pulse profiles, which are more readily observed at low radio frequencies (typically in the range 100

to 1000 MHz) where the pulsar is known to be bright and (b) accurate time alignment of the multi-frequency pulse profiles. As we now describe, the GMRT, because of some unique features, offers a novel way for obtaining accurate DM estimates.

The GMRT is a multi-element aperture synthesis telescope (Swarup et al. 1997) consisting of 30 antennas, distributed over a region of 25 km diameter, which can also be configured as a “single dish” in the incoherent or coherent array mode (Gupta et al. 2000). Furthermore, it supports a “sub-array” mode of operation where different sets of antennas can be configured completely independently to produce more than one single dish. Thus, the same pulsar can be observed simultaneously at more than one radio band.

The GMRT operates at radio frequencies in the range 150 MHz to 1400 MHz with observing bands available at 150, 235, 325, 610 and 1400 MHz. The antennas can be grouped into several sub-arrays and each sub-array can independently be operated at a radio band of interest, thus enabling simultaneous multi-frequency observations. Signals from different observing frequency bands and antennas are eventually down-converted to baseband signals of 16 MHz band-width. The signals are subsequently sampled at the Nyquist rate and processed through a digital receiver system consisting of a correlator and a pulsar back-end.

For each antenna, operating at a given frequency band, the pulsar back-end receives signals in 256 channels spanning the band-width of 16 MHz, for each of two orthogonal polarizations. The relative delay – geometrical as well as instrumental – between different antenna signals is compensated to an accuracy of 32 nanosec before they reach the pulsar receiver. The corresponding signals from selected antennas (say from one sub-array) can be added together incoherently by the pulsar receiver.

For this experiment, the signals from antennas in all sub-arrays were added incoherently in the same pulsar receiver, to produce a single stream of output data, which was recorded at a sampling rate of 0.516 millisecond. Because of the dispersive delay between the different radio bands of observation, the pulse arrives at different times (and hence, at different pulse phases) at each frequency band. This fact is utilised to separately extract the streams of single pulses at each frequency band, from the single stream of recorded data, during the offline analysis. This scheme eliminates the need for having separate, but synchronised, pulsar receiver chains for each sub-array and also does away with any requirement of accuracy of absolute time stamping of the recorded data – the data from the different sub-arrays is naturally synchronised. Since all known instrumental and geometric delays have been corrected for all the sub-arrays, the residual arrival time delay between pulses from different radio bands of observation is only and entirely due to the dispersion delay. This allows the DM to be measured to a very high degree of accuracy.

There is, however, one drawback of the above scheme. In order to recover the pulsed signal for the different frequency bands during off-line analysis, dispersion delays across the 256 channels (16 MHz baseband band-width) for each frequency band are computed and the data are collapsed to obtain a time series for each band. In this process, however, the data from the other frequency band are wrongly de-dispersed and appear as a smeared out signal producing

Table 1. Relevant parameters of our selected sample of pulsars.

Pulsar	Catalog DM (pc/cm ³)	Period (sec)	S ₄₀₀ (mJy)	Distance (kpc)	V _{pm} (km s ⁻¹)	Duration of scan (min)	Frequency combination of observation (MHz)
B0329+54	26.776	0.7145	1650	1.43	145	33	227-243 + 610-626
B0818-13	40.99	1.2381	100	2.46	376	22	227-243 + 325-341
B0823+26	19.4751	0.5307	65	0.38	196	22	227-243 + 325-341
B0834+06	12.8579	1.2738	85	0.72	174	22	227-243 + 325-341
B0950+08	2.9702	0.2531	400	0.12	21	22	325-341 + 610-626
B1133+16	4.8471	1.1877	300	0.27	475	33	325-341 + 610-626
B1642-03	35.665	0.3877	300	2.90	660	11	325-341 + 610-626
B1642-03	35.665	0.3877	300	2.90	660	11	227-243 + 325-341
B1919+21	12.4309	1.3373	200	0.66	122	11	227-243 + 325-341
B1929+10	3.176	0.2265	250	0.17	86	11	227-243 + 325-341
B1929+10	3.176	0.2265	250	0.17	86	22	325-341 + 610-626
B2016+28	14.176	0.5579	320	1.10	12	11	227-243 + 314-320
B2016+28	14.176	0.5579	320	1.10	12	22	325-341 + 610-626
B2045-16	11.51	1.9616	125	0.64	289	11	227-243 + 314-320
B2217+47	43.54	0.5385	135	2.45	375	22	325-341 + 610-626

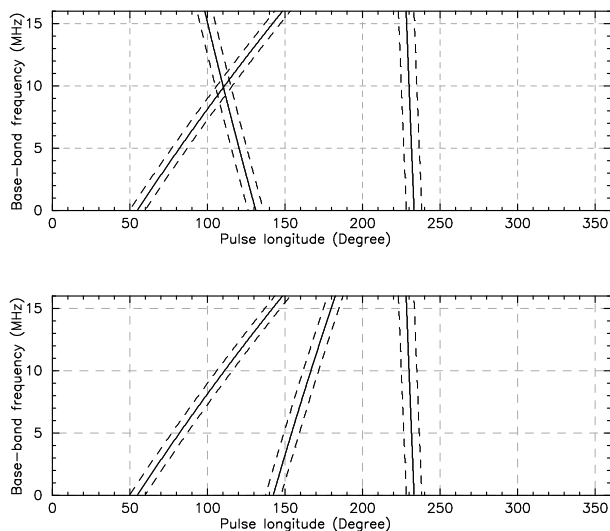


Figure 1. Dispersion curves across the 16 MHz of base-band signal for pulsar B2016+28. The upper panel shows (left to right) the dispersion curves for the 243 to 227, 325 to 341 and 610 to 626 MHz bands of observation & the lower panel shows the dispersion curves for 243 to 227, 320 to 304 and 610 to 626 MHz bands, respectively. The dotted curves on both sides of the continuous curves delineate the extent of the 50% width of the average profile.

excess undesired power in the off-pulse region. In some cases this may overlap with the on-pulse signal from the desired frequency band, resulting in corruption of the data. Thus, in order to obtain undistorted signals, it is essential that we choose an observing strategy that avoids such overlaps. This requires us to examine the detailed nature of the DM delay curve at each frequency band of interest, and to ensure that the curves do not intersect each other within the 16 MHz of baseband band-width. In Figure 1 we show an example of this. Here, the upper panel (from left to right) shows the dispersion curves for pulsar B2016+28 in the frequency bands 243 to 227, 325 to 341 and 610 to 626 MHz, as

seen in the base-band signal, after removal of all delays that are integer multiple of the pulsar period. It shows that the two dispersion curves at frequency bands 243-227 MHz and 325-341 MHz intersect with one another over certain range of channels. Hence, this combination of frequency bands can not be used for such observations of this pulsar. By suitably changing the value of the local oscillator signals used for the down conversion of the radio frequency bands to base-band signals, the range as well as the direction of the radio frequency signals that span the 16 MHz band-width can be changed, thus ensuring proper separation of the dispersion curves. In this particular case, it has been achieved by moving the local oscillator such that the 325 MHz band covers 320 to 304 MHz (see lower panel of Figure 1). Appropriate frequency combinations were found for each pulsar in our sample.

For this experiment, we selected a sample of 12 pulsars having sufficiently large fluxes ($S_{400} > 100$ mJy), a range of DM values ($\sim 10 - 40$ pc/cm³), and sampling different directions in the Galaxy. The relevant parameters are summarised in Table 1, where columns 2,3,4,5 and 6 give the values of the DM, period, flux at 400 MHz, distance and proper motion respectively, as obtained from the pulsar catalog of Taylor, Manchester & Lyne (1993). At every epoch of observation, each pulsar from our sample was observed for a few thousand pulses (column 7 gives the duration of the observing scan) at a pair of frequency bands (given in column 8 of Table 1) selected from the available bands of the GMRT. The epochs were separated by intervals of about two weeks, and the whole experiment was carried out over a duration of about one and half years.

3 DATA REDUCTION AND ESTIMATION OF DM

The recorded data were pre-processed off-line to convert from raw time-frequency format to a single pulse time series and folded profiles. The pre-processing involved de-

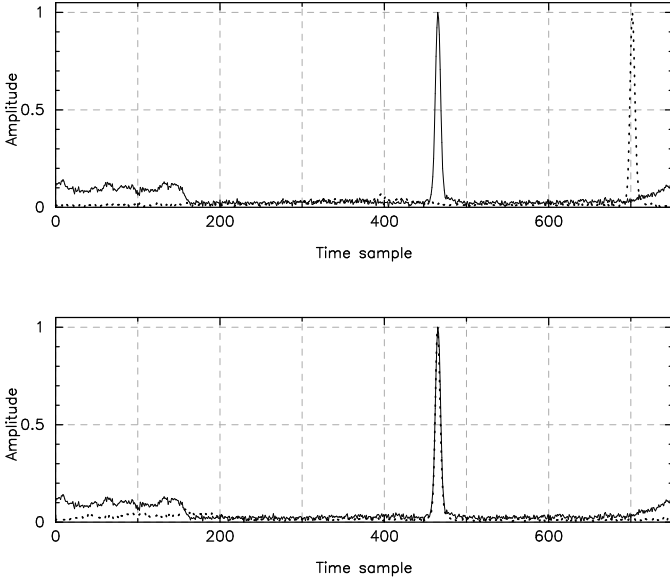


Figure 2. Average pulse profiles of the pulsar B1642–03 observed at 610 (solid curve) + 325 (dotted curve) MHz bands combination. The upper and lower panels show the pulse profiles before and after the alignment respectively. The excess power regions near both edges of the profile at 610 MHz are examples of wrongly de-dispersed data from the other band.

dispersion of the data in two frequency bands, folding and interference rejection.

For each pulsar, to recover the pulse trains at the two radio bands, the acquired data were de-dispersed within the 16 MHz band-width of each band by using the catalog DM values given in Table 1. Where needed, bad data points were rejected from the de-dispersed data. For this, after masking the data from the on-pulse regions, the running mean data from the off-pulse regions was computed and subtracted from the original data. Next, off-pulse data points with amplitude greater than the threshold value (typically chosen as 3 times the off-pulse RMS) were flagged. In addition, data were scanned visually, and manual editing of bad data due to radio frequency interference was carried out, where needed. At the end of the data rejection step, if a large fraction of the data around any on-pulse window was found to be bad, the entire pulse was flagged.

The de-dispersed, interference free data trains were folded at the Doppler-corrected pulsar periods to obtain the average pulse profiles at the two radio frequency bands (see Figure 2 for an example). The pulse profile data at each observation band were demarcated with three windows – two off-pulse and one on-pulse window. The on-pulse window contained the properly de-dispersed average pulse profile, while the off-pulse windows (one on each side of the on-pulse) were off-pulse regions which were free of contamination from the wrongly de-dispersed pulse profile of the other frequency band. Data only from these window regions were used in the subsequent analysis described below.

From the reduced data, the dispersion delay between the two frequency bands was estimated and, using Equation 2, the corresponding DM value was obtained. For these calculations, Doppler corrected frequencies f_1 and f_2 (with

$f_1 > f_2$) were used, with these frequencies being related to the frequencies of observations, f_{1m} and f_{2m} , through

$$f_1 = f_{1m} \sqrt{\frac{1+\beta}{1-\beta}} \quad \text{and} \quad f_2 = f_{2m} \sqrt{\frac{1+\beta}{1-\beta}}, \quad \beta = \frac{v_{net}}{c}; \quad (5)$$

where v_{net} is the radial velocity of the observer with respect to the pulsar, which is predominantly due to the orbital motion of the earth around the Sun. Similarly, the value of Δt in Equation 2 needs to be the measured topocentric delay, Δt_m , corrected to the solar system barycenter, as follows:

$$\Delta t = \Delta t_m \times (1 - \beta) \quad . \quad (6)$$

The total measured time delay, Δt_m , can be expressed as a sum of three terms:

$$\Delta t_m = \Delta t_p + \Delta t_i + \Delta t_f \quad , \quad (7)$$

where Δt_p is the integral number of pulsar periods delay, Δt_i is the number of time sample bins delay within a pulsar period and Δt_f is the fraction of a time sample bin delay. The value of Δt_m can be estimated by two different techniques: (i) by estimating the delay between the average pulse profiles, and (ii) by measuring the mean delay between the single pulse data trains. We have carried out the analysis using both these methods, and the steps for each are described below.

As the first step, the data were reduced to zero mean off-pulse sequences. In the average profile (hereafter AP) method, the mean from the off-pulse data windows was estimated and subtracted from the whole pulse profile data. In the single pulse (hereafter SP) method, the mean computation and baseline subtraction was carried out individually for each pulse, while using the same off-pulse windows.

In the AP method, because of the folding process, the value of Δt_p can not be directly estimated from the folded profiles; instead, it was estimated from the knowledge of the frequencies for the two bands, the catalog DM value and the pulsar period. To estimate Δt_i , pulse profiles at the two frequency bands were cross-correlated, and the integer time sample lag at which the cross-correlation peaked was taken as value of Δt_i . The lower frequency pulse profile was rotated left circularly by this amount to align it with the higher frequency pulse profile (see Figure 2 for an example).

The cross-correlation (hereafter CC) of the pulse profiles at two given frequencies (see Figure 3 for an example) can be given as,

$$CC(kT) = \sum_{n=1}^N f(nT)g(nT - kT). \quad (8)$$

Here, $CC(kT)$ is the CC for k^{th} bin shift of the pulse profile at the lower frequency, N is the number of time sample bins within an on-pulse window, and f and g are the pulse profiles at two observation frequencies. In the SP method, the two time series were cross-correlated, and the peak of cross-correlation function gave the time delay with an accuracy of a time sample bin. In this method, the CC could be started from zero shift of the lower frequency pulse profile, but to reduce unnecessary computations, we started CC computations from a shift equivalent to the number of time sample bins corresponding to Δt_p . During the cross-correlation computations in both the methods, care was taken to ensure that data points from the wrongly de-dispersed signals

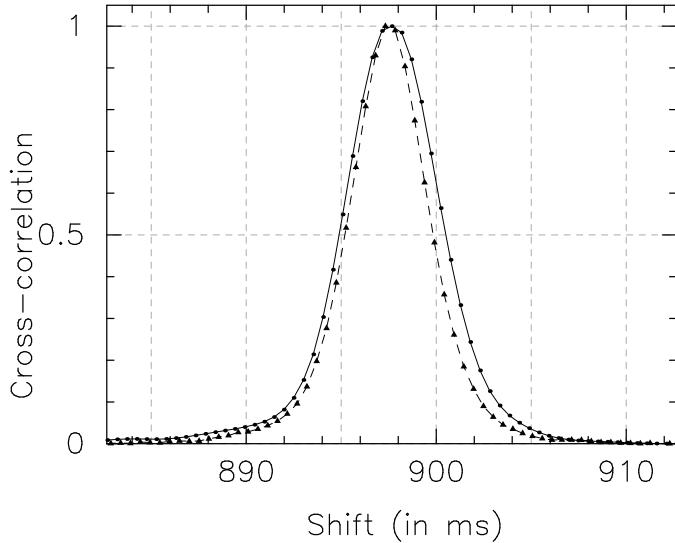


Figure 3. The normalized cross-correlation function (CCF) for pulsar B1642–03 observed at 610+325 MHz bands. The continuous curve shows the CCF for average pulse profiles and dashed one correspond to single pulse analysis.

were not included in the computations. This was done by using data points from the above defined on-pulse and off-pulse windows only, and restricting the lag range to values which ensured no overlap of these windows with wrongly de-dispersed data points.

The average profile is obtained by folding the time series data at the pulsar period. Since individual pulses show significant pulse to pulse jitter in the longitude of occurrence, the average profile is usually significantly broader than the individual pulses. As a result the CCF obtained in the AP analysis is broader in comparison to that from the SP analysis (e.g. Figure 3). In the AP method, the CCF reflects the sum of cross-correlation of all pulses at one radio band with all pulses from the other band, while in the SP analysis, the CCF is the sum of the CC between corresponding pulses at the two radio bands. Therefore, one can expect the DM delay estimated by the two methods to be different, as we find in our results.

The precision of DM measurement mainly depends on the accuracy in estimating the time delay between two pulse profiles. The CC as described above gives an accuracy of the order of an integral time sample bin. To estimate the delay with an accuracy of a fraction of a time sample bin, the cross-spectrum (CS) was computed and a linear gradient was fitted to the phase of the CS. Let us first consider the AP method. If the two pulse profiles are $f(t)$ and $g(t)$, then their Fourier transforms (FT) can be written as,

$$f(t) \iff F(\nu) = |F(\nu)|e^{i(\phi_{1i} + 2\pi\nu t_{1f})} \quad (9)$$

and

$$g(t) \iff G(\nu) = |G(\nu)|e^{i(\phi_{2i} + 2\pi\nu t_{2f})} ; \quad (10)$$

where $|F(\nu)|$ and $|G(\nu)|$ are the amplitudes of Fourier transform components at the transform frequency ν , t_{1f} and t_{2f} are the positions of the peaks of the two pulse profiles from their reference points of Fourier transformation in the time

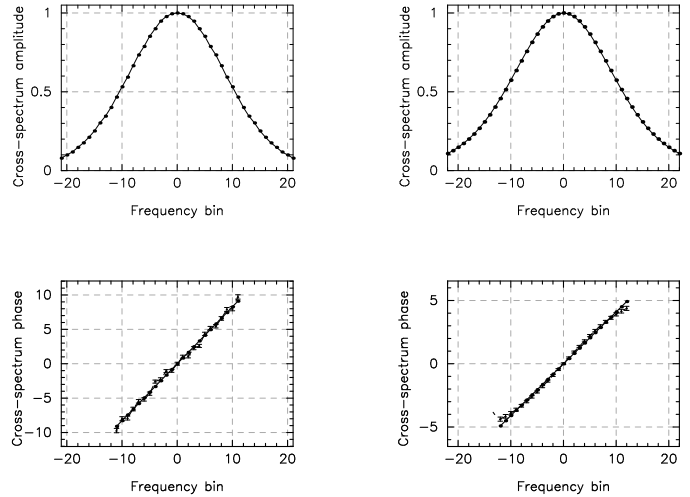


Figure 4. Normalized CS amplitude (upper panels), and CS phase with error bars (lower panels) of average profiles (left side panels) and single pulses (right side panels) for pulsar B1642–03, at one epoch observed at 610+325 MHz bands. The straight line in the phase plot is the best fit linear gradient.

domain, and ϕ_{1i} and ϕ_{2i} are the intrinsic phases of the two pulse profiles. The cross-spectrum can then be written as,

$$CS(\nu) = F(\nu)G^*(\nu) = |F(\nu)||G(\nu)|e^{-i\phi_{CS}(\nu)} ; \quad (11)$$

where the phase $\phi_{CS}(\nu)$ is given by

$$\phi_{CS}(\nu) = \phi_{2i} - \phi_{1i} + 2\pi\nu\Delta t_f , \quad (12)$$

with $\Delta t_f = t_{2f} - t_{1f}$ the fractional time sample bin delay.

For $\phi_{1i}(\nu) = \phi_{2i}(\nu)$, i.e. when the pulse profiles at the two frequencies have the same shape, the effect of a fractional bin delay will show up as a linear gradient in the phase plot of the CS (see Figure 4), given by

$$\Delta t_f = \frac{\Delta\phi_{CS}}{2\pi\Delta\nu} . \quad (13)$$

The cross-spectrum can be obtained from the Fourier transformation of the CCF or from the product of the individual Fourier transformations. Of the two we have preferred the latter for the AP method, as this helps in the proper propagation of errors from time domain to frequency domain, as explained below. In the SP analysis, however, we have used the Fourier transformation of the CCF, with an appropriate strategy for computing the errors in the final DM results.

Let us now look at the estimation of the error in the measured delay, which is primarily due to the finite signal to noise ratio of the data. For the AP method, the noise in the folded profiles, estimated from the off-pulse windows, was properly propagated to the CS. For each pulse profile, the RMS of phase, $\sigma_{\phi(\nu)}$, and amplitude, $\sigma_{A(\nu)}$, of the Fourier transform can be estimated as,

$$\sigma_{\phi(\nu)} = \sigma_t \sqrt{\frac{N}{2(Im_{\nu}^2 + Re_{\nu}^2)}} , \quad (14)$$

$$\sigma_{A(\nu)} = \sigma_t \sqrt{\frac{N}{2}} . \quad (15)$$

Here N is the number of data points used for fast Fourier

transformation (FFT), Im_ν and Re_ν are real and imaginary parts respectively of the Fourier components at frequency bin ν , and σ_t is the RMS of the off-pulse noise. The RMS of the CS phase, $\sigma_{\phi_{CS}(\nu)}$, was computed by adding the noise from the two phases in quadrature,

$$\sigma_{\phi_{CS}(\nu)}^2 = \sigma_{\phi_1(\nu)}^2 + \sigma_{\phi_2(\nu)}^2 \quad (16)$$

In the SP method, the RMS obtained from off-pulse windows was properly propagated to estimate the RMS at each point of the CCF. The greatest value of this RMS was used as a conservative estimate in Equation 14 to estimate the RMS of the CS phase. After this step, the procedure for estimating the error in the DM was the same for the AP and SP methods.

The phase gradient, $\nabla(\phi_{CS})$, was computed as the slope of the best fitted line, $\nabla(\text{bestfit})$, obtained by the least-square method. Thus,

$$\Delta t_f = \frac{\nabla(\text{bestfit}) \times N_{FFT} \times T}{360} \quad (17)$$

where N_{FFT} is the number of data points used to compute the FFT and T is the time sample. The RMS of Δt_f was estimated as

$$\sigma_{\Delta t_f} = \frac{\sigma_{\nabla(\text{bestfit})} \times N_{FFT} \times T}{360} \quad (18)$$

Because the error in Δt estimation was only due to $\sigma_{\Delta t_f}$, the error in the final DM value was given by

$$\sigma_{DM(\text{noise})} = \frac{\sigma_{\Delta t_f}}{\Delta t_c} DM \quad (19)$$

The above steps were carried out at each epoch to obtain a time series of DM values for each pulsar (see Figure 5 for example).

4 RESULTS AND DISCUSSIONS

The results obtained for the average profile method are summarised in Table 2. Here, column 2 gives the catalog DM value for each pulsar from Taylor, Manchester & Lyne (1993), and the observing frequency bands are given in column 3. For each pulsar, we obtained the mean dispersion measure over the period of observations, $\langle DM \rangle$, and the quadrature average of $\sigma_{DM(\text{noise})}$, using:

$$\langle DM \rangle = \frac{\sum_{i=1}^{N_{ep}} DM_i}{N_{ep}} \quad (20)$$

$$\sigma_{DM(\text{noise})}^2 = \frac{\sum_{i=1}^{N_{ep}} \sigma_{DM_i(\text{noise})}^2}{N_{ep}} \quad (21)$$

where DM_i and $\sigma_{DM_i(\text{noise})}$ are the measured dispersion measure and the RMS dispersion at the i^{th} epoch, and N_{ep} is the total number of epochs of observations (column 4 of Table 2). The quantity $\sigma_{DM(\text{noise})}$ (column 6 of Table 2) gives the average of the DM error bar estimate from all epochs of observations. This quantity gives an estimate of the contribution to the total RMS fluctuation seen in the time series, due to sources of error in the DM estimate. The values for $\sigma_{DM(\text{noise})}$ for most pulsars are such that the DM estimate is accurate to 1 part in 10^4 or better.

We also estimated the total fluctuation of the DM time series, $\sigma_{DM(\text{total})}$ (column 7 of Table 2), as

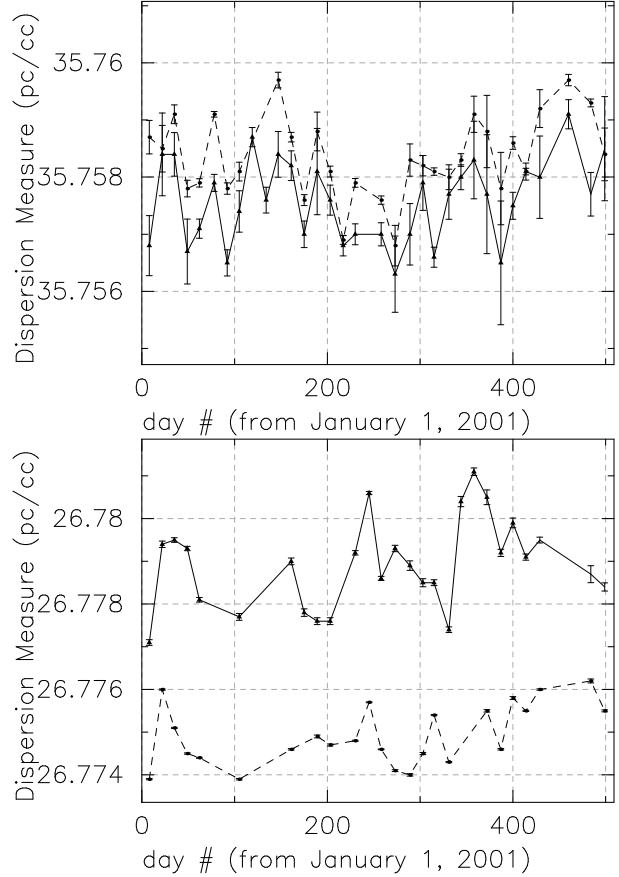


Figure 5. Variation of DM with time for pulsars B1642–03 (upper panel) and B0329+54 (lower panel) observed at frequencies 610+325 MHz and 610+243 MHz respectively, over the interval 08 Jan 2001 to 14 May 2002, as a function of day number. The continuous line shows the results from average profile analysis, and the dotted one from single pulse analysis. The error bars are $3\sigma_{DM(\text{noise})}$ values.

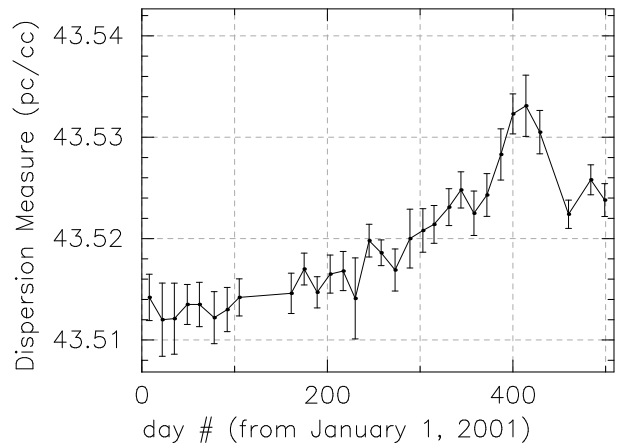


Figure 6. DM variation with $3\sigma_{DM(\text{noise})}$ error bars for pulsar B2217+47 observed at frequencies 610+325 MHz, over the time interval 08 Jan 2001 to 14 May 2002 as a function of day number. The catalog value of the DM is 43.54 pc/cm³.

Table 2. DM results from average profile analysis

Pulsar	Catalog DM (pc/cm ³)	Frequency combination (MHz)	N_{ep}	$\langle DM \rangle$ (pc/cm ³)	$\sigma_{DM(noise)}$ (pc/cm ³)	$\sigma_{DM(total)}$ (pc/cm ³)	$\Delta DM/\sigma_{DM(total)}$ (pc/cm ³)
B0329+54	26.776	243 + 610	26	26.77870	0.00003	0.00103	+ 2.64
B0818-13	40.99	243 + 325	32	40.9222	0.0013	0.0043	- 15.71
B0823+26	19.4751	243 + 325	29	19.4545	0.0004	0.0016	- 12.85
B0834+06	12.8579	243 + 325	29	12.8671	0.0004	0.0017	+ 5.38
B0950+08	2.9702	325 + 610	31	2.9597	0.0008	0.0050	- 2.1
B1133+16	4.8471	325 + 610	34	4.8288	0.0006	0.0071	- 2.57
B1642-03	35.665	325 + 610	33	35.75760	0.00014	0.00072	+128.20
B1642-03	35.665	243 + 325	34	35.72270	0.00007	0.00090	+ 64.00
B1919+21	12.4309	243 + 325	32	12.4445	0.0011	0.0054	+ 2.50
B1929+10	3.176	243 + 325	31	3.1755	0.0004	0.0015	- 0.31
B1929+10	3.176	325 + 610	27	3.1750	0.0004	0.0020	- 0.51
B2016+28	14.176	243 + 320	29	14.1611	0.0007	0.0025	- 6.07
B2016+28	14.176	325 + 610	30	14.1664	0.0008	0.0051	- 1.90
B2045-16	11.51	243 + 320	31	11.5094	0.0012	0.0114	- 0.05
B2217+47	43.54	325 + 610	31	43.5196	0.0007	0.0061	- 3.38

$$\sigma_{DM(total)} = \sqrt{\frac{\sum_{i=1}^{N_{ep}} (DM_i - \langle DM \rangle)^2}{N_{ep}}} . \quad (22)$$

In the most general case, this total RMS of the DM fluctuation is composed of a part due to estimation error on the DM (Equation 21) and the remaining due to other processes likely to play a role in the time variability of DM (a prime candidate for which is DM fluctuation due to large scale electron density irregularities in the ISM). An estimate of the variance due to such processes can be obtained as

$$\sigma_{DM(ISM)}^2 = \sigma_{DM(total)}^2 - \sigma_{DM(noise)}^2 . \quad (23)$$

As can be seen in columns 6 and 7 of Table 2, for almost all the pulsars, $\sigma_{DM(noise)}$ is much smaller than $\sigma_{DM(total)}$, indicating the presence of substantial DM fluctuations due to such sources. We return to this aspect in more detail at the end of this section.

4.1 On the constancy of $\langle DM \rangle$ estimates

Keeping in mind the total RMS for each DM estimate ($\sigma_{DM(total)}$), we can see that the mean DM, $\langle DM \rangle$, for each pulsar is estimated with a fairly good accuracy – ~ 1 part in 10^3 or better (DM accuracy at each epoch is ~ 1 part in 10^4). It is interesting to compare these mean DM values with other estimates in literature. Column 8 of Table 2 shows the difference between our $\langle DM \rangle$ value and the catalog DM value (Taylor, Manchester & Lyne 1993), in units of $\sigma_{DM(total)}$. While for most pulsars our results agree with the catalog values within $3 \sigma_{DM(total)}$, there are some pulsars, namely B0818-13, B0823+26, B0834+06, B1642-03 and B2016+28, which show a significant difference. We now discuss these discrepant cases in some detail, using for comparison results from (i) the old pulsar catalog of Taylor, Manchester & Lyne (1993) (ii) the new pulsar catalog (Hobbs et al. 2004, see also www.atnf.csiro.au/research/pulsar/psrcat), and (iii) other reports in literature.

For pulsar B0818-13 we find a $\langle DM \rangle$ of $40.922 \pm$

0.004 pc/cm^3 , which is significantly smaller than the value of $40.99 \pm 0.03 \text{ pc/cm}^3$ given in the old catalog, which comes from a very early measurement (Manchester & Taylor 1972). It is interesting to note that Kuzmin et al. (1998) find an intermediate value of 40.965 pc/cm^3 for this pulsar, from measurements made between 1984 and 1991. Furthermore, the new pulsar catalog gives a value of $40.938 \pm 0.003 \text{ pc/cm}^3$ (Hobbs et al. 2004), which is intermediate between that of Kuzmin et al. (1998) and our result. One interesting possibility from the above data points is that the DM of this pulsar is showing a slow and secular decline with time, on time scales of decades.

For pulsar B0823+26 we again find a mean DM that is significantly smaller than the value in the old catalog (based on the work of Phillips & Wolszczan (1992)). Our result is also discrepant from that of Kuzmin et al. (1998), which is in good agreement with the old catalog value. However, the new pulsar catalog (Hobbs et al. 2004) cites value of $19.454 \pm 0.004 \text{ pc/cm}^3$, which is fully consistent with our result.

For pulsar B0834+06 we find a $\langle DM \rangle$ ($12.867 \pm 0.002 \text{ pc/cm}^3$) that is somewhat larger than the old catalog value of $12.8579 \pm 0.0002 \text{ pc/cm}^3$ (based on the work of Phillips & Wolszczan (1992)). For this pulsar, Kuzmin et al. (1998) report a value of 12.865 pc/cm^3 , which agrees quite well with our result, whereas the new pulsar catalog (Hobbs et al. 2004) cites a value of 12.889 pc/cm^3 , significantly higher than all the other numbers for this pulsar.

For B2016+28, our $\langle DM \rangle$ values (from 2 different pairs of frequencies) are consistent with each other, but are significantly smaller than the results cited in the old catalog (based on the work of Craft (1970)), the new catalog (based on the work of Hobbs et al. (2004)), as well as in Kuzmin et al. (1998), all of which are consistent with each other.

Amongst all our results, the mean value of DM for PSR B1642-03 shows the largest discrepancy with the original catalog value of $35.665 \pm 0.005 \text{ pc/cm}^3$ (based on very early work of Hunt (1971)). This is true for our DM re-

sults from both sets of frequency pairs, though the discrepancy is more for our results obtained from measurements at 325 + 610 MHz bands (the difference in DM values from the two frequency pairs is discussed separately in the next subsection). We note that the DM of 35.73 pc/cm³ obtained by Kuzmin et al. (1998) is equally discrepant from this catalog value, and lies in between our two estimates. A similar value (35.737 ± 0.003 pc/cm³) is obtained from a multi-frequency timing analysis of over 30 years of data for this pulsar by Shabanova et al. (2001). The new pulsar catalog gives a value of 35.727 ± 0.003 pc/cm³ (Hobbs et al. 2004), very close to the lower of our two results. Clearly, either the original value of the DM reported for this pulsar was erroneously estimated, or there has been a significant evolution of the DM of this pulsar from the early years of its discovery.

PSR B1642–03 is a particularly interesting pulsar, in several other respects. There is a significant uncertainty in the distance estimate to this pulsar. The dispersion measure derived distance is 2.9 kpc (with an uncertainty of 50%), whereas the neutral hydrogen measurements provide a distance constraint of 160 pc (lower limit) (Graham et al. 1974). The smaller distance to this pulsar is also supported by a model (by Prentice and ter Haar 1969) that ascribes much of the DM to the presence of the H_{II} region ζ Oph. along the line of sight. Furthermore, Shabanova et al. (2001) find that this pulsar has a very small proper motion and estimate transverse velocities of 2 and 30 km/s for the two distance estimates. In addition, Shabanova et al. (2001) also claim evidence for free precession in this pulsar, based on their analysis of the timing data.

Some of the above properties have interesting connections with the DM results. For example, Gupta et al. (1994) show that the observed scintillation properties of this pulsar are consistent with a line of sight that goes through the limb of an H_{II} region. In such a case, a long term systematic variation of the pulsar DM would be expected if there was sufficient transverse relative motion between the pulsar and the H_{II} region. However we see no evidence for such a variation in our data. On the other and, the observed DM changes could be part of a cyclic DM variation on large time scales, such as corresponding to the precession period (\sim few 1000 days). For example, results from the multi-frequency timing data of Shabanova et al. (2001) show timing residuals at two different frequencies (\sim 0.1 GHz and 0.6–2.3 GHz) which have differences between them that vary as a function of phase in the precession cycle. The maximum amplitude of this difference is \sim 1 ms, implying that the 0.1 GHz pulses arrive \sim 1 ms later than the pulses at higher frequencies, at these phases. One possible explanation of these variations is a cyclic change in DM of $\sim 2.5 \times 10^{-3}$ pc/cm³. This, however, is too small compared to the changes and variations seen between the different DM values reported above. Thus, although there is a lot more information about this pulsar, the nature and reason for the observed DM variations does not come out clearly.

From the results in this subsection, it is clear that constancy of DM estimates (at the level of 1 part in 1000 or better) for a pulsar can not be taken for granted. Whether these small changes are due to genuine temporal evolution of pulsar DMs or due to differences in the estimation techniques, remains to be established.

4.2 DM values from different pairs of frequency bands

For two of our pulsars – B1642-03 and B2016+28 – we carried out the observations at two pairs of frequency bands. These data are almost simultaneous in that the observations at each epoch were taken within an hour or so of each other, and hence can be compared with each other. PSR B1642–03 was observed at the frequency pairs of 325 + 610 MHz and 243 + 325 MHz and we find a significant difference in the mean DM values from these two sets of data (Table 2). The value obtained from the higher frequency combination (325+610 MHz) is higher than that obtained from the lower frequency combination (243+325 MHz). On the other hand, for B2016+28 the DMs obtained from the two frequency pairs (325 + 610 MHz and 243 + 320 MHz) are the same within errors, as determined by $\sigma_{DM_{(total)}}$.

Though it is generally thought that the DM value for a pulsar is independent of the frequency of measurement, there have been reports in literature about differences in pulsar DMs that have been estimated from different parts of the radio spectrum (e.g. Shitov et al. (1988); Hankins (1991)). In most of these results, the evidence is for an excess delay in the arrival of the pulses at low frequencies, when attempting to align them with a DM value computed from the higher frequencies. However, our results for PSR B1642–03, albeit for a relatively narrow range of radio frequencies, show an opposite trend in that the DM value is larger for the higher frequency pair (325 + 610 MHz).

There are different possible explanations for frequency dependent DM variations. For example, an evolution in the shape of the profile with frequency can play a role in changing the inferred alignment between the profiles at two different frequencies. This should play a more significant role for pulsars with complex, multi-component profiles, but should be relatively insignificant for pulsars with simple profiles (such as pulsars B1642–03 and B2016+28 in our sample). Another interesting possibility is an extra time delay between emission received at two frequencies due to different heights of emission of these frequencies in the pulsar magneto-sphere (e.g. Kardashev et al. 1982), an idea that has not received much attention in the past. These aspects will be examined in greater detail in a separate, forthcoming paper.

4.3 DM differences from average profiles and single pulses

As described in section 3, the DM estimates were obtained from two independent methods: measurement of delays between the average profiles (the AP method; results reported in Table 2) and measurement of delays between single pulse trains (the SP method). We find, in general, that the DM results for a pulsar depend on the method of analysis. For some pulsars, this difference is negligible, e.g. PSR B1642–03 (see Figure 5). For others it is significant: PSR B0329+54 is one such example in our study (see lower panel of Figure 5) – the $\langle DM \rangle$ value obtained from the SP analysis is 26.7751 ± 0.0007 pc/cm³, which is significantly lower than the catalog value, which in turn is lower than the $\langle DM \rangle$ value from the AP analysis.

It is worth noting that dispersion measure values es-

timated from alignment of average profiles and those from cross-correlation of single pulse emission features have been reported to be different in the past also. Hankins (1991) found that DM values from average profile measurements are significantly larger than those obtained from cross-correlation of pulsar micro-structure, for PSR B0950+08 and PSR B1133+16. Stinebring et al. (1992) have also investigated results for PSR B1133+16 over a ten year period, obtained using different techniques, and found significant variations in the DM values.

Further, as described in section 3, these two methods actually measure slightly different quantities. Thus, the difference between average profile and single pulse analysis results that we find is not so surprising. A detailed description of these results and an investigation into the possible causes and implications of the same will be taken up in another forthcoming paper.

4.4 Slow fluctuations of pulsar DMs

As mentioned at the beginning of this section, there is evidence for substantial temporal fluctuations in DM values for most of the pulsars. A large part of this is likely to be due to the ISM. A detailed study of this aspect will be taken up separately in another forthcoming paper. Here, we briefly comment on the variations observed, comparing them with earlier published results.

Variations in pulsar DM, by definition, can arise due to either spatial and temporal changes in the electron density along the line of sight, or change in the distance to the pulsar, or both. Electron density changes along the line of sight to the pulsar can be in the form of fluctuations resulting in DM fluctuations; alternatively, there can be a monotonic increase (or decrease) in DM due to the pulsar sampling a gradient of the electron density. Most of our observed DM fluctuations (except PSR B2217+47) show fluctuations over a constant mean DM, indicating that the observed changes are due to electron density fluctuations in the ISM. In the case of temporal change of distance to the pulsar with respect to the observer, the effect would manifest only as monotonic increase or decrease in pulsar DM. In our sample, PSR B2217+47 shows a monotonic increase of its DM (Figure 6). However, the amplitude of this change ($\simeq 0.02$ pc/cm³/year) is such that it would require a very large radial velocity ($\sim 10^6$ km/s) through a normal density ISM (~ 0.02 /cm³), or a very high density ISM (~ 200 /cm³) for normal pulsar velocities (~ 100 km/s). It is likely that the cause for this change is due to the pulsar sampling an electron density gradient in the ISM, rather than due to radial motion of the pulsar.

Such an electron density gradient can be produced by the line of sight to the pulsar crossing through a blob of enhanced plasma density. Taking the electron density enhancement of Δn_e pc/cm³ in a wedge of thickness L pc, the observed change in DM is $\Delta DM = \Delta n_e \cdot L$. The pulsar's transverse displacement X (of $\sim 3 \times 10^{-4}$ pc), samples this electron density gradient in one year. Assuming the wedge to be part of a spherical blob of radius L pc (and $X \sim L$), we can estimate the electron density gradient to be $\sim 2 \times 10^5$ /cm³/pc or 1 /cm³/AU. This value is a lower limit – if the cloud is closer to the observer, the electron density gradient could be even higher. Evidence

for such AU-size clouds of enhanced electron density in the ISM also comes from scintillation observations of pulsars. For example, Bhat et al. (1999) find evidence for clouds with length scales of ~ 10 AU and electron density contrast \sim a few electrons/cm³. Our results are similar, though a bit on the higher side.

Long term, slow DM variations, on time scales of weeks to months, have been studied in the past by Backer et al. (1993) (3 pulsars) and Phillips & Wolszczan (1991) (6 pulsars). Whereas Backer et al. (1993) report total DM fluctuations ~ 0.02 pc/cm³ over 1 – 2 year periods, Phillips & Wolszczan (1991) report typical variations ~ 0.002 pc/cm³ (and smaller) over similar time intervals. Our results show $\sigma_{DM(total)} \sim 0.001$ to 0.007 pc/cm³ for most cases, implying total fluctuations ~ 0.005 to 0.03 pc/cm³. These are typically larger than those reported by Phillips & Wolszczan (1991), but comparable to the results of Backer et al. (1993).

4.5 Summary

We have presented a new experiment for accurate measurement of pulsar DMs using the GMRT in a simultaneous, multi-frequency sub-array mode. We have shown that single epoch DM estimates using this technique can achieve an accuracy of 1 part in 10^4 or better. With improved sensitivity performance of the GMRT and faster sampling that is now available, this accuracy can be improved in future experiments and the technique can be extended to a larger set of pulsars. From the large number of epochs of DM measurements for each of the 12 pulsars in our sample, we are able to obtain fairly accurate estimates for the mean DM for most of them. A detailed comparison of DM values in the literature with our mean DM values highlights the lack of consistency (at the level of ~ 1 part in 1000) in the different DM estimates, the reason for which remains to be understood. We have also briefly highlighted some of the other results from our data – such as DM estimates from different frequency combinations, differences in average profile and single pulse DM values, and slow fluctuations of pulsar DMs with time (which are most likely to be due to ISM effects) – these will be the subject of follow-up papers.

Acknowledgments :

We thank the staff of the GMRT for help with the observations. The GMRT is run by the National Centre for Radio Astrophysics of the Tata Institute of Fundamental Research. We thank V. Kulkarni and R. Nityananda for help and encouragement during the initial stages of this work. YG would like to acknowledge the help of P. Gothoskar in the devising of the original experiment.

REFERENCES

- Backer, D. C., Hama, S., Hook, S. V., and Foster, R. S., 1993, *ApJ* **404**, 636.
- Bartel, N., Kardashev, N. S., Kuzmin, A. D., Nikolaev, N. Ya., Popov, M. V., Sieber, W., Smirnova, T. V., Soglasnov, V. A., and Wielebinski, R., 1981, *A&A*, **93** 85.
- Bhat, N.D.R., Gupta, Y., Rao, P., 1999, *ApJ* **514**, 249.
- Craft, H. D., 1970, *PhD thesis*, **Cornell University**.

- Graham, D.A., Mebold, U., Hesse, K.H., Hills, D.L., Wielebinski, R., 1974, *A&A* **37**, 405.
- Gupta, Y., Rickett, B. J., Lyne, A. G., 1994, *MNRAS* **269**, 1035.
- Gupta, Y., Gothoskar, P. B., Joshi, B. C., Vivekanand, M., Swain, R., Sirothia, S., and Bhat, N.D.R., 2000, in IAU Colloq. 177, Pulsar Astronomy, ed. M. Kramer, N. Wex, and R. Wielebinski (ASP Conf. Ser. 202; San Francisco: ASP), 277.
- Hankins, T.H. , 1987, *ApJ* **312**, 276.
- Hankins, T. H., Izvekova, V. A., Malofeev, V. M., Rankin, J. M., Shitov, Y. P., and Stinebring, D. R., 1991, *ApJ* **373**, L17.
- Hobbs, G., Lyne, A. G., Kramer, M., Martin, C. E. and Jordan, C. A., 2004, *MNRAS* **353**, 1311.
- Hunt, G. C., 1971, *MNRAS* **153**, 119.
- Kardashev, N. S., Nikolaev, N. Ya., Novikov, A. Yu., Popov, M. V., Soglasnov, V. A., Kuzmin, A. D., Smirnova, T. V., Bartel, N., Sieber, W., and Wielebinski, R., 1982, *A&A*, **109** 340.
- Kuzmin, A. D., Izvekova, V. A., Shitov, Yu. P., Sieber, W., Jessner, A., Wielebinski, R., Lyne, A. G., Smith, F. G., 1998, *A&A Suppl. Ser.* **127**, 355.
- Manchester, R. N., and Taylor, J. H., 1972 *Ap Lett.* **10**, 67.
- Phillips, J. A. and Wolszczan, A., 1991, *ApJ* **382**, L27.
- Phillips, J. A. and Wolszczan, A., 1992, *ApJ* **385**, 273.
- Prentice, A.J.R., Haar, D. ter, 1969, *MNRAS* **146**, 423.
- Shabanova, T.V., Lyne, A.G., Urama, J.O., 2001, *ApJ* **552**, 321.
- Shitov, Yu. P., Malofeev, V. M. and Izvekova, V. A., 1988, *Sov. Astron. Lett.* **14(3)**, 181.
- Stinebring, D.R., Thorsett, S. E., and Kaspi, V. M., 1992, in IAU Colloq. 128, ed. Hankins, T.H., Rankin, J.M., Gil, J.A., (Poland: Pedagogical University Press), 349.
- Swarup, G., Ananthakrishnan, S., Subrahmanya, C. R., Rao, A. P., Kulkarni, V. K., and Kapahi, V. K., 1997, in High Sensitivity Radio Astronomy, ed. N. Jackson and R. J. Davis (Cambridge: Cambridge University Press).
- Taylor, J. H., Manchester, R. N., and Lyne, A. G., 1993, *ApJS* **88**, 529.